Validity of the Effective Medium Theory for Modeling Near-Field Thermal Emission by Nanowire Arrays

Saman Zare, Ramin Pouria, and Sheila Edalatpour

Department of Mechanical Engineering, University of Maine, Orono, ME 04469, USA

ABSTRACT

Nanowire arrays are promising man-made materials for tuning the spectrum and the magnitude of near-field thermal radiation. Near-field radiative properties of nanowire arrays are often studied using the effective medium theory (EMT). In this paper, we inspect the validity of the Maxwell-Garnett (MG) and Bruggeman (BR) EMTs for predicting near-field thermal emission by quartz and indium tin oxide (ITO) nanowire arrays. The near-field energy density predicted using the EMTs is compared with numerical simulations obtained using the thermal discrete dipole approximation. For quartz nanowire arrays, which support localized surface phonons in the infrared region, neither MG nor BR EMT can accurately predict the spectrum and the magnitude of near-field thermal emission even at distances, z_0 , greater than the array pitch, L over π . Based on the performed simulations, the EMT agrees the best with the T-DDA when $1 < \frac{L}{z_0} < \pi$. It is also shown that MG EMT is slightly more consistent with numerical simulations than the BR EMT. For the ITO array, which does not support localized surface plasmons in the infrared region, the MG EMT provides an acceptable estimations of near-field thermal radiation. Finally, it is observed that near-field emission can vary by a factor of two in lateral directions which cannot be captured in the EMT.

Keywords: Nanowire arrays, Effective medium theory, Maxwell-Garnett model, Bruggeman model, Thermal discrete dipole approximation

I. INTRODUCTION

Man-made materials engineered at the sub-wavelength scale (the dominant wavelength of thermal radiation at room temperature is about 10 µm) offer great potential for tuning the magnitude and the spectrum of near-field thermal emission. A class of man-made materials that has attracted significant attention is nanowire arrays. Nanowire arrays can support hyperbolic modes resulting in a broadband enhancement of thermal emission as well as surface phonons resulting in sharp (narrow-band) peaks in the spectrum of the emitted energy. So far, near-field thermal emission by nanowire arrays has been mostly studied using the effective medium theory (EMT) [1-19]. In this theory, the nanowire array is modeled as an anisotropic (uniaxial), homogeneous film with effective parallel (to the optical axis which is along the nanowires axis) and perpendicular dielectric functions determined from those of the nanowires and the free space. Maxwell-Garnett (MG) [20-22] and Bruggeman (BR) [21-23] EMTs are used for determining the effective dielectric function. The EMT is assumed to be valid for in the long wavelength regime (i.e., when the nanowires and the array pitch are much smaller than the thermal wavelength in the free space) and at observation distances greater than the array pitch divided by π [1,11,13,15,18]. Although the validity of the EMT for modeling near-field thermal radiation of man-made materials such as multilayer media [24-33], gratings [34-38], nanoparticles on a flat surface [39-41], and nanoholes [42-43] has been investigated, the applicability of the EMT to nanowire arrays has not been thoroughly inspected. Mirmoosa et al. [44] studied the validity of the EMT for modeling metallic nanowires and concluded that the EMT can be used qualitatively for predicting the magnitude of the radiative heat transfer. In this study, the transverse-magnetic (TM) polarized transfer function (instead of radiative heat transfer) was calculated using ANSYS HESS and compared with the EMT for a few frequencies and parallel components of the wavevector, k_{ρ} , smaller than the

wavevector in the substrate. As such, the validity of the EMT for predicting near-field thermal emission integrated over all k_{ρ} modes and the near-field spectrum (and thus the location of the peaks and hyperbolic bands) was not analyzed. Yu et al. [43] studied how radiative heat transfer between a bulk Drude emitter and a bulk gallium antimonide (semiconductor) absorber is affected if the surface of the absorber is patterned into nanowires. It was found that the EMT can only qualitatively predict the spectral locations of the peaks in the radiative heat transfer, and it cannot provide an accurate estimation of the magnitude of heat transfer even when the size of the nanowires is smaller than the wavelength. However, the validity of the EMT for modeling near-field thermal radiation of nanowire-array emitters made of dielectric and metallic materials is still unverified.

In this paper, the validity of the MG and BR EMTs for modeling near-field thermal emission by periodic arrays of quartz and indium tin oxide (ITO) nanowires is investigated by comparing these models against the thermal discrete dipole approximation (T-DDA) simulations. The T-DDA is a numerically exact solution of the Maxwell equations augmented by the thermally fluctuating current given by the fluctuation dissipation theorem [45]. Near-field emission by arrays with various filling factors, nanowire heights and diameters at different perpendicular and lateral observation distances is considered. Quartz nanowire arrays support both hyperbolic and surface phonon-polariton modes in the infrared portion of the electromagnetic spectrum, where these modes can be thermally excited. The ITO nanowires do not support surface plasmon-polariton and hyperbolic modes in the infrared region.

This paper is structured as follows. The problem under consideration, the MG and BR EMTs, and the T-DDA approach for modeling periodic arrays are presented in Section II. The EMT results

for the energy density are compared with the T-DDA simulations in Section III, and the concluding remarks are provided in Section IV.

II. Near-field thermal emission by periodic arrays of nanowires

A. Description of the problem

A schematic of the problem under consideration is shown in Fig. 1(a). A periodic array of nanowires is at temperature T and emits in the free space. The nanowires have a diameter of D, a height of H, and they are separated by a gap of size d such that the array has a pitch of L = D + d. The energy density thermally emitted by the array at observation point $\mathbf{r_0} = (x_0, y_0, z_0)$ is desired.

B. Effective medium theory

In the effective medium theory, the periodic array of the nanowires is modeled as a homogenous film with an anisotropic effective dielectric function as shown in Fig. 1(b). Two EMTs, namely Maxwell-Garnett (MG) and Bruggeman (BR) EMTs, are commonly used for finding the effective dielectric function of the homogenized thin film.

The MG EMT is derived by assuming the nanowires as single dipoles. This assumption is valid only in the quasi-static regime, i.e., when the nanowires are much smaller than the wavelength in the free space, the wavelength in the nanowires, the interwire spacing, and the observation distance. Then, the total dipole moment of the array due to illumination of an external field, \mathbf{E}^{ext} , is obtained by summing up the dipole moment of the individual nanowires, i.e.,

$$\mathbf{p}_{\alpha}^{tot} = N_{w} \alpha_{w,\alpha} \mathbf{E}^{ext} \tag{1}$$

where the subscript α refers to the direction ($\alpha = \| \text{ or } \bot$) with respect to the optical axis of the nanowire array, $\mathbf{p}_{\alpha}^{tot}$ is the total dipole moment of the array in direction α , N_w is the number of

the nanowires in the array, and $\alpha_{w,\alpha}$ is the nanowire polarizability in direction α [22]. Equation 1 is obtained by assuming that the external incident field is the same for all nanowires. This assumption is only valid in the long-wavelength regime (i.e., when $L \ll \lambda_v$ with λ_v being the wavelength in the free space) where it can be assumed that the phase of the external field remains constant. An effective electric susceptibility, $\chi_{eff,\alpha}$, can be assigned to the nanowire array and is found as [46]:

$$\chi_{eff,\alpha} = \frac{\mathbf{p}_{\alpha}^{tot}/V}{\mathbf{E}_{\alpha}^{in}} \tag{2}$$

where V is the volume of the array, $\mathbf{p}_{\alpha}^{tot}/V$ is the average electric polarization of the array, and \mathbf{E}_{α}^{in} is the average electric field inside the array. Substituting Eq. 2 into Eq. 1 results in:

$$\chi_{eff,\alpha} = \frac{\alpha_{w,\alpha}}{V_{uc}} \frac{\mathbf{E}^{ext}}{\mathbf{E}_{\alpha}^{in}} \tag{3}$$

where $V_{uc} = V/N_w$ is the volume of the unit cell of the array. For finding the effective susceptibility of the array using Eq. 3, a relation between the external and internal fields should be established. Assuming negligible interactions between the nanowires, the electric field inside the array is given by [22]:

$$\mathbf{E}_{\alpha}^{in} = \left(1 - \frac{4\pi g_{\alpha}}{\varepsilon_{\nu}} \frac{\alpha_{w,\alpha}}{V_{uc}}\right) \mathbf{E}^{ext} \tag{4}$$

where $\varepsilon_{v} = 1$ is the dielectric function of the free space, and g_{α} is the geometry-dependent depolarization factor for cylindrical nanowires in direction α . The depolarization factor g_{α} in Eq. (4) can be calculated as [47]:

$$g_{\perp} = \frac{1}{2}\cos\theta - i\frac{k_v^3}{6\pi}V_w \tag{5a}$$

$$g_{\parallel} = 1 - \cos\theta - \frac{k_{\nu}^{2}}{6\pi} V_{w} C_{z} - i \frac{k_{\nu}^{3}}{6\pi} V_{w}$$
 (5b)

where *i* is the imaginary unit, k_v is the magnitude of the wavevector in the free space, $\theta = \tan^{-1}(D/H)$, $V_w = \pi H D^2/4$ is the volume of a nanowire, and $C_z = \frac{3}{2H} ln \left| \frac{1+E}{1-E} \right|$ with $E = 1 + \left(\frac{D}{H} \right)^2$ [47].

Equation 4 is only valid for very dilute arrays as it is obtained by assuming negligible interaction between nanowires. Using Eq. 4 and substituting for the polarizability of the nanowires ($\alpha_{w,\alpha} = \frac{vV_w}{4\pi} \frac{\varepsilon_v(\varepsilon_w - \varepsilon_v)}{\varepsilon_v + g_\alpha(\varepsilon_w - \varepsilon_v)}$, where ε_w is the dielectric function of the nanowires [22]), the effective susceptibility of the array in Eq. 3 can be written as:

$$\chi_{eff,\alpha} = \frac{1}{4\pi} \frac{f\varepsilon_v(\varepsilon_w - \varepsilon_v)}{\varepsilon_v + g_\alpha(1 - f)(\varepsilon_w - \varepsilon_v)} \tag{6}$$

The parameter f in Eq. 6 is the filling factor of the array given by $f = \frac{V_w}{V_{uc}}$. The effective dielectric function of the array is related to the susceptibility as $\varepsilon_{eff,\alpha} = \varepsilon_v + 4\pi \chi_{eff,\alpha}$ [46]; thus, the effective dielectric function can be found as:

$$\varepsilon_{eff,\alpha} = \varepsilon_v + f \frac{\varepsilon_v(\varepsilon_w - \varepsilon_v)}{\varepsilon_v + g_\alpha(1 - f)(\varepsilon_w - \varepsilon_v)}$$
(7)

Equation 7 is referred to as the MG EMT. The MG EMT suffers from the shortcoming that it is not symmetric with respect to the inclusions and the host medium [21,22]. In other words, if the array is assumed as free-space holes in a host medium made of the same material as the nanowires, a different effective dielectric function is found compared to the case where nanowires are assumed

as inclusions in a free-space host medium. This asymmetry of the effective dielectric function is particularly drastic when the difference between the filling factors or the dielectric functions of the two media is large [21,22].

In the BR EMT, the nanowires and the free-space medium are treated in a symmetrical manner. However, this does not mean that the BR EMT is more accurate the MG EMT [22]. The BR EMT is obtained by embedding the nanowire array in an infinite medium with the same dielectric function as the effective film. If the infinite medium and the nanowire array have the same dielectric function, the polarization of the nanowire array should be zero. The BR formula can be obtained by replacing the dielectric function of the host medium in the generalized MG formula (i.e., the formula generalized to account for more than one inclusion) by the effective dielectric function [21,22]:

$$f\frac{\varepsilon_w - \varepsilon_{eff,\alpha}}{\varepsilon_{eff,\alpha} + g_{\alpha}(\varepsilon_w - \varepsilon_{eff,\alpha})} + (1 - f)\frac{\varepsilon_v - \varepsilon_{eff,\alpha}}{\varepsilon_{eff,\alpha} + g_{\alpha}(\varepsilon_v - \varepsilon_{eff,\alpha})} = 0$$
(8)

An explicit expression for the BR effective dielectric function cannot be obtained. In this case, Eq. (8) can be written as the following quadratic equation:

$$(1 - g_{\alpha})\varepsilon_{eff,\alpha}^{2} + [(g_{\alpha} - f)\varepsilon_{w} - (1 - f - g_{\alpha})]\varepsilon_{eff,\alpha} - g_{\alpha}\varepsilon_{w} = 0$$
(9)

The solution of Eq. (9) that results in a non-negative value for the imaginary part of $\varepsilon_{eff,\alpha}$ is selected as the effective dielectric function.

Once the effective dielectric function is found, the energy density, u, emitted by the anisotropic thin film can be calculated at distance z_o above the film in the free space as [48]:

$$u(\omega, T) = \frac{\Theta(\omega, T)}{4\pi^2 \omega} \left(k_v^2 \int_0^{k_v} \frac{k_\rho}{|k_{z,v}|} \sum_{\gamma = TE, TM} (1 - |R^{\gamma}|^2 - |T^{\gamma}|^2) dk_\rho + 2 \int_{k_v}^{\infty} \frac{k_\rho^3}{|k_{z,v}|} \sum_{\gamma = TE, TM} Im[R^{\gamma}] e^{-2|k_{z,v}|z_o} dk_\rho \right)$$
(10)

where ω is the angular frequency, Θ is the mean energy of an electromagnetic state, k_{ρ} is the parallel (to the film interface) component of the wavevector, and $k_{z,v}$ is the perpendicular component of the wavevector in the free space. In Eq. (10), R^{γ} and T^{γ} represent the reflection and transmission coefficients of the film for γ -polarization (γ = transverse electric (TE) or magnetic (TM)), respectively, and are calculated as [49]:

$$R^{\gamma} = \frac{r_{vf}^{\gamma} + r_{fv}^{\gamma} e^{2iHk_{z,f}^{\gamma}}}{1 + r_{vf}^{\gamma} r_{fv}^{\gamma} e^{2iHk_{z,f}^{\gamma}}}$$
(11a)

$$T^{\gamma} = \frac{t_{vf}^{\gamma} t_{fv}^{\gamma} e^{iHk_{z,f}^{\gamma}}}{1 + r_{vf}^{\gamma} r_{fv}^{\gamma} e^{2iHk_{z,f}^{\gamma}}}$$
(11b)

where the subscript f and v correspond to the film and the free space, respectively, and $k_{z,f}^{\gamma}$ is the perpendicular component of the wavevector in the film for γ -polarization which is given by [25]:

$$k_{z,f}^{TE} = \sqrt{\varepsilon_{eff,\perp} k_v^2 - k_\rho^2} \tag{12a}$$

$$k_{z,f}^{TM} = \sqrt{\varepsilon_{eff,\perp} k_v^2 - \frac{\varepsilon_{eff,\perp}}{\varepsilon_{eff,\parallel}} k_\rho^2}$$
 (12b)

The parameters r_{ij}^{γ} and t_{ij}^{γ} in Eq. (11) are respectively the Fresnel reflection and transmission coefficients at the interface of layers i and j for γ -polarization. The Fresnel coefficients are given by [25]:

$$r_{ij}^{TE} = \frac{k_{z,i}^{TE} - k_{z,j}^{TE}}{k_{z,i}^{TE} + k_{z,j}^{TE}}$$
(13a)

$$r_{ij}^{TM} = \frac{\varepsilon_{j,\perp} k_{z,i}^{TM} - \varepsilon_{i,\perp} k_{z,j}^{TM}}{\varepsilon_{j,\perp} k_{z,i}^{TM} + \varepsilon_{i,\perp} k_{z,j}^{TM}}$$

$$\tag{13b}$$

$$t_{ij}^{TE} = \frac{2k_{z,i}^{TE}}{k_{z,i}^{TE} + k_{z,j}^{TE}}$$
 (13c)

$$t_{ij}^{TM} = \frac{2\varepsilon_{j,\perp} k_{z,i}^{TM}}{\varepsilon_{j,\perp} k_{z,i}^{TM} + \varepsilon_{i,\perp} k_{z,j}^{TM}} \sqrt{\frac{\varepsilon_{j,\perp}}{\varepsilon_{j,\parallel}}}$$
(13d)

It should be noted that the free space is an isotropic medium, and thus $\varepsilon_{v,\perp} = \varepsilon_{v,\parallel} = \varepsilon_v$ and $k_{z,v}^{TE} = k_{z,v}^{TM} = k_{z,v}$.

C. Thermal discrete dipole approximation

Numerical simulations of thermal emission by the nanowire array is done using the periodic thermal discrete dipole approximation (T-DDA) [50-52]. The periodic T-DDA requires discretizing only one period of the array, and thus is computationally practicable. In this method, a nanowire, referred to as the unit cell, is discretized into N cubical sub-volumes. The sub-volumes should be much smaller than the nanowires (D and H), their separation distance (d), the observation distance (z_0), and the wavelength (λ). In this case, the variation of the electric field within the sub-volumes is negligible such that the sub-volumes behave as electric point dipoles. The array can be constructed by replicating the unit cell along the x- and y-directions. The replicas

of the unit cell are numbered as (m, n), where m and n show the row and the column number of a replica, respectively. The energy density at the observation point \mathbf{r}_o due to thermal emission by the nanowire array can be calculated using the electric and magnetic dyadic Green's functions of the array as [52]:

$$u(\mathbf{r}_o, \omega) = \frac{2k_v^2}{\pi\omega} \sum_{j=1}^N V_j \varepsilon'' \Theta(\omega, T) \sum_{m=0}^{N_{kx}} \sum_{n=0}^{N_{ky}} \operatorname{Trace}[k_v^2 \mathbf{G}_{jmn,o}^E \otimes \mathbf{G}_{jmn,o}^E + \mathbf{G}_{jmn,o}^H \otimes \mathbf{G}_{jmn,o}^H]$$
(14)

where V_j is the volume of sub-volume j, ε^n is the imaginary part of the dielectric function of the nanowires, \otimes is the outer product, $N_{k\beta}$ ($\beta = x, y$) is the number of mathematical wave vectors selected for discretizing the Brillouin zone along β -direction, the subscript o refers to the observation point, and the subscript jmn refers to replica (m, n) of the sub-volume j in the unit cell. Additionally, $\mathbf{G}_{jmn,o}^{E(H)}$ represents the dyadic electric (magnetic) Green's function of the array which relates the electric (magnetic) field at the observation point \mathbf{r}_o to the thermally generated fluctuating current at sub-volume jmn. The dyadic Green's function of the array can be obtained by integrating the wavevector-dependent Green's function over the Brillouin zone as [52]:

$$\mathbf{G}_{jmn,o}^{\xi} = \frac{L^2}{(2\pi)^2} \int_{-\frac{\pi}{L}}^{\frac{\pi}{L}} \int_{-\frac{\pi}{L}}^{\frac{\pi}{L}} \mathbf{g}_{jmn,o}^{\xi} (k_x, k_y) dk_y dk_x, \quad \xi = E \text{ or } H$$
 (15)

where $\mathbf{g}_{jmn,o}^{\xi}$ is the wavevector-dependent Green's function of the array between sub-volume jmn and the observation point. The Green's function $\mathbf{g}_{jmn,o}^{\xi}$ is only phase shifted relative to $\mathbf{g}_{j00,o}^{\xi}$. As such, $\mathbf{g}_{jmn,o}^{\xi}$ can be related to $\mathbf{g}_{j00,o}^{\xi}$ as [52]:

$$\mathbf{g}_{jmn,o}^{\xi} = \mathbf{g}_{j00,o}^{\xi} e^{i(mLk_x + nLk_y)}, \qquad m, n = 0, \pm 1, \pm 2, \dots, j = 1, 2, 3, \dots, N$$
 (16)

where $\mathbf{g}_{j00,o}^{\xi}$ is found by solving the following system of equations [52]:

$$\frac{1}{\alpha_{i}}V_{j}\varepsilon_{v}(\varepsilon-1)\mathbf{g}_{j00,o}^{\xi}-k_{v}^{2}\sum_{l=1}^{N}V_{l}(\varepsilon-1)\mathbf{G}_{j,l}^{0E,P}.\mathbf{g}_{l00,o}^{\xi}=\mathbf{G}_{j,o}^{0\xi,P}, j=1,2,3,...,N$$
(17)

where α_j is the polarizability of sub-volume j, ε_v is the free space permittivity, and $\mathbf{G}_{j,l}^{0\xi,P}$ represents the periodic free-space dyadic Green's function between sub-volume j in the unit cell and point l (where l refers to either the observation point or a sub-volume in the unit cell). The periodic free-space dyadic Green's function between j and l, $\mathbf{G}_{j,l}^{0\xi,P}$, is defined as [53]:

$$\mathbf{G}_{j,l}^{0\xi,P} = \sum_{m=-\infty}^{\infty} \sum_{n=-\infty}^{\infty} \mathbf{G}_{j00,lmn}^{0\xi} e^{i(mLk_x + nLk_y)}$$
(18)

In Eq. (18), $\mathbf{G}_{j00,lmn}^{0\xi}$ is the free-space dyadic Green's function between sub-volume j in the unit cell and the point lmn (i.e., the replica (m,n) of point l). By substituting Eq. (18) into Eq. (17) and solving the system of equations, $\mathbf{g}_{j00,o}^{\xi}$ is found. Then, using $\mathbf{g}_{j00,o}^{\xi}$ and Eqs. (14)-(15), the energy density emitted by the periodic array of nanowires is calculated.

III. RESULTS

Thermal emission by periodic arrays of quartz and ITO nanowires is considered. Based on the EMT, quartz nanowires support both surface and hyperbolic modes, while thermal emission by ITO nanowires does not exhibit any resonances. The non-approximate simulations of the energy density are done using the periodic T-DDA, and the results are compared with those predicted by MG and BR EMTs. The periodic T-DDA and the EMT results are compared for different perpendicular and lateral observation distances, filling factors, and nanowire heights and diameters.

A. Comparison of the EMT with the T-DDA for various perpendicular observation distances and filling factors

The energy density emitted by three arrays of quartz nanowires is considered. The arrays all have a diameter D of 100 nm and a height H of 20 nm, while they have different nanowire spacings. The nanowires are separated by a distance d of 200 nm in the first array, 62 nm in the second array, and 20 nm in the third one. The filling factor f of these arrays is 0.09, 0.30, and 0.55, respectively, such that they correspond to a dilute, a medium-density, and a dense array. The energy density for each array is calculated at three perpendicular observation distances z_o of 20 nm ($L/z_o > \pi$), 100 nm ($L/z_o < \pi$), and 500 nm ($L/z_o < \pi$) above the array on the central axis of the nanowires (i.e., at $x_o = y_o = 0$). The arrays are emitting at a temperature T of 400 K.

The energy density emitted by the array with f=0.09 is shown in Fig. 2(a). The real part of the effective dielectric function of the array in the parallel ($\varepsilon'_{eff,\parallel}$) and perpendicular ($\varepsilon'_{eff,\perp}$) directions as predicted using the MG and BR EMTs is also shown in Fig. 2(b). As it is seen from Fig. 2(b), the MG and BR EMTs predict different values for $\varepsilon'_{eff,\parallel}$ in the spectral band of 1000-1141 cm⁻¹ and for $\varepsilon'_{eff,\perp}$ in the spectral band of 1168-1244 cm⁻¹, where quartz has metallic behavior ($\varepsilon'<0$). Based on the MG EMT, the array has a hyperbolic band ($\varepsilon'_{eff,\parallel}\cdot\varepsilon'_{eff,\perp}<0$) at 1101-1122 cm⁻¹, while the BR EMT does not predict any hyperbolic thermal emission for the array. The energy densities predicted by the MG and BR EMTs do not agree in the spectral band of 1000-1222 cm⁻¹. Neither of EMTs can accurately predict the magnitude and the spectrum of the energy density. The EMT models underestimate the total (spectrally-integrated) energy density by a factor of ~ 7 at $z_0=20$ nm and a factor of ~ 2.6 at $z_0=100$ nm, while they overestimate the energy density at $z_0=500$ nm by a factor of ~ 1.4 . The spectrum of the energy density as predicted

using the EMT has several peaks, and it remains almost the same when the observation distance increases from 20 nm to 500 nm. The energy density emitted by the effective film is dominated by the contribution of transverse-magnetic (TM) polarized electromagnetic waves, and it resonantly increases when $\text{Im}[r^{TM}]$ is maximum. In the quasistatic limit (i.e., when $k_{\rho} \gg k_{0}$), $\text{Im}[r^{TM}] \approx 2\text{Im}\left[\varepsilon_{eff,\parallel}/\varepsilon_{eff,\parallel}/\varepsilon_{eff,\parallel}/\varepsilon_{eff,\parallel}/\varepsilon_{eff,\parallel}/\varepsilon_{eff,\parallel}/\varepsilon_{eff,\parallel}\right]^{2}$. Peaks in the EMT energy density are observed at wavenumbers for which $\text{Im}\left[\varepsilon_{eff,\parallel}/\varepsilon_{eff,\parallel}/\varepsilon_{eff,\parallel}/\varepsilon_{eff,\perp}\right]$ has local maxima or when $\varepsilon_{eff,\parallel} \to -\sqrt{\varepsilon_{eff,\parallel}/\varepsilon_{eff,\perp}}$. The peaks at 697, 801, 1163, and 1225 cm⁻¹ in the MG and BR EMT spectra are due to the former condition, while the high energy density around 1110 cm⁻¹ in the MG spectrum is due to hyperbolic thermal emission in the spectral range of 1101 – 1122 cm⁻¹.

Unlike the EMT, the T-DDA predicts distance-dependent spectra for the energy density. At $z_o = 20$ nm, the T-DDA spectrum of the energy density is almost the same as that for a single nanowire. This is because the observation distance is much smaller than the array pitch $(L/z_o = 15)$ such that the energy density is mostly dominated by the contribution of the single nanowire located directly below the observation point. Also, thermal emission by the single nanowire is very similar to that for a thin film of quartz (rather than a film with effective dielectric function) with a thickness equal to the height of the array except for in the spectral range of 1090-1153 cm⁻¹ where the dipole mode of the nanowire resonantly emits. The nanowire below the observation point acts similar to a thin film since its diameter is much greater than the observation distance $(D/z_o = 5)$. The peaks in the T-DDA energy density are located at 699 cm⁻¹, 807 cm⁻¹, 1110 cm⁻¹, 1153 cm⁻¹, 1181 cm⁻¹, 1197 cm⁻¹. These peaks except for the one at 1110 cm⁻¹ can be accurately predicted by modeling the wire as a thin film of quartz. The peak at 1110 cm⁻¹ is associated with the dipole mode of the nanowire. The nanowire can be modeled as an oblate spheroidal dipole with semi-axes equal to 50

nm (D/2) and 10 nm (H/2). Thermal emission by the nanowire is proportional to the imaginary part of the polarizability of the spheroidal dipole given by $\text{Im}[\alpha_j] = \varepsilon_v V \varepsilon'' / |1 + L_j(\varepsilon - 1)|^2$ where L_j is the geometrical factor of the spheroid along j-direction (j = x, y, z) [54]. When $\varepsilon =$ $(L_j - 1)/L_j$, $\text{Im}[\alpha_j] \to \infty$ and thermal emission by the dipole resonantly increases due to the excitation of localized surface phonons (LSPhs). The peak at 1110 cm⁻¹ is associated with the resonant polarizability along the x- and y-directions. At $z_0 = 100$ nm, the energy density is still similar to that for a single nanowire since L/z_o is large $(L/z_o = 3)$. However, the nanowire cannot be considered as a film of quartz anymore as D and z_o are comparable ($D/z_o=1$). At $z_o=500$ nm, where the distance is greater than the pitch size of the array ($L/z_o=0.6$), the cumulative effect of the nanowires becomes significant such that the spectrum of the energy density cannot be predicted using the one for a single nanowire anymore. In this case, the energy density by the array is about an order of magnitude larger than that for a single nanowire. Figure 2(a) shows that none of the EMTs can accurately model the cumulative thermal emission by the nanowires, even though it is assumed that the EMT is valid when $L/z_o < \pi$. The EMTs significantly overestimate the energy density at $z_o = 500$ nm. Among the two EMTs, the MG EMT spectrum agrees more with the T-DDA at $z_o = 500$ nm. Nevertheless, the difference between the MG EMT and the T-DDA is non-negligible. It should also be mentioned that the hyperbolic thermal emission in the spectral band of 1101 – 1122 cm⁻¹ which is predicted by the MG EMT is not observed in the T-DDA energy density. Instead, the T-DDA energy density in this spectral band peaks at 1110 cm⁻¹ due to the excitation of the LSPhs.

The EMT is compared with the T-DDA for a larger filling factor of f = 0.30 in Fig. 2(c). The real part of the effective dielectric function in the parallel and perpendicular directions predicted by the MG and BR EMTs is shown in Fig. 2(d). Based on the MG EMT, the array has two wide hyperbolic

bands at 1095 - 1151 cm⁻¹ and 1200 - 1225 cm⁻¹. The BR EMT predicts one hyperbolic band at 1072 - 1133 cm⁻¹. The T-DDA energy density at $z_0 = 20$ nm is still very similar to a single nanowire since the observation distance is much smaller than the array pitch ($L/z_o=8.1$). The MG EMT energy density at $z_0 = 20$ nm shows a broadband hyperbolic thermal emission around 1127 cm⁻¹, while the BR EMT displays a hyperbolic emission around 1092 cm⁻¹. This disagrees with the T-DDA energy density at $z_0 = 20$ nm where thermal emission is dominated by the contribution of the LSPh mode of the single nanowire in this spectral band. At $z_o = 100$ nm ($L/z_o = 1.6$) and 500 nm $(L/z_o = 0.3)$, the T-DDA energy density deviates from that for the single nanowire. At these two distances, the cumulative thermal emission by the nanowires enhances the energy density particularly at the LSPh resonance wavenumber. The cumulative thermal emission at $z_0 = 100$ nm is captured well using the MG EMT expect for in the spectral band of 1000 - 1244 cm⁻¹ where quartz has mostly metallic behavior. The MG EMT does not agree with the T-DDA at $z_0 = 500$ nm as for the case with f = 0.09. It should also be mentioned that the EMT spectra do not show broadband emissions at $z_0 = 100$ nm and 500 nm since the number of contributing hyperbolic modes decreases with the distance as z_0^{-2} [1].

The filling factor of the array is further increased to f = 0.55 in Fig. 2(e). The real part of the effective dielectric function predicted using the MG and BR EMTs is shown in Fig. 2(f). The T-DDA energy density at $z_o = 20$ nm ($L/z_o = 6$) does not vary significantly with increasing the filling factor, and it is still very similar to that for a single nanowire. The BR EMT has a broad hyperbolic band from 1072 cm⁻¹ to 1230 cm⁻¹ resulting in a broadband thermal emission at this spectral region. The MG EMT has three hyperbolic bands causing enhanced thermal emission around 1142 cm⁻¹, 1170 cm⁻¹ and 1205 cm⁻¹. This is while the T-DDA energy density at $z_o = 20$ nm, which is dominated by the contribution of only one nanowire, does not show any hyperbolic emission. At

 $z_o = 100$ nm ($L/z_o = 1.2$) and 500 nm ($L/z_o = 0.24$), the T-DDA energy density is significantly affected by the collective contribution of the nanowires such that the energy density increases by factors of 2.2 and 40.2, respectively, relative to the one for a single nanowire at the same distance. Similar to the case of f = 0.30, the MG EMT agrees the most with the T-DDA at $z_o = 100$ nm while deviating significantly from the T-DDA for $z_o = 500$ nm.

B. Effect of height

The validity of the EMT is tested against the T-DDA for quartz nanowires of greater height in this sub-section. The nanowires height is increased by one order of magnitude from 20 nm to 200 nm, while the diameter of the nanowires is kept at 100 nm. The energy density emitted by an array with f = 0.3 (d = 62 nm) is shown in Fig. 3(a) for two observation distances of $z_0 = 100$ nm ($L/z_0 = 100$ nm) 1.6) and 500 nm ($L/z_0 = 0.3$). The real part of the effective dielectric function of the array is also shown in Fig. 3(b). The BR EMT predicts a hyperbolic band of 1075 cm⁻¹ – 1133 cm⁻¹ for the array, while the array has two hyperbolic bands at 1098 cm⁻¹ – 1147 cm⁻¹ and 1176 cm⁻¹ – 1197 cm⁻¹ based on the MG EMT. Single nanowires of the same height and diameter support a sharp LSPh peak at 1110 cm⁻¹. However, this peak is not observed in the T-DDA energy density of the array. Instead, the T-DDA energy density shows a broadband behavior around this wavenumber at $z_0 = 100$ nm and does not show any enhancement at $z_0 = 500$ nm (the contribution of hyperbolic modes decays with distance as z_0^{-2}). Comparing the EMT and T-DDA energy densities in Fig. 3(a), the same conclusions as for the array with H = 20 nm can be made about the accuracy of the EMT. The MG EMT agrees more with the T-DDA than BR EMT. The best agreement is obtained for $z_o = 100$ nm ($L/z_o = 1.6$), and both EMTs greatly overestimate thermal emission at $z_o = 500$ nm $(L/z_o = 0.3)$.

C. Effect of lateral observation distance

In the EMT, it is assumed that the energy density emitted by the array is uniform along the x- and y-directions. To verify this assumption, the energy density emitted by an array of quartz nanowires with D = 100 nm, H = 200 nm, and f = 0.30 at a distance of $z_o = 100$ nm (for which the EMT agrees the most with the T-DDA) is calculated at three values of x_o equal to 0 nm, 50 nm, and 81 nm using the T-DDA. The T-DDA results are compared to the MG and BR EMT predictions in Fig. 4. The simulations are done for $y_o = 0$. It is seen from the T-DDA simulations that the locations of the peaks in the energy density spectra remain the same as x_o increases. However, the hyperbolic emission around 1110 cm⁻¹ decreases with increasing x_o . Additionally, the magnitude of the energy density decreases by a factor of 2 as x_o increases from 0 nm to 81 nm. Clearly, these effects are not captured in the EMT energy density.

D. Effect of diameter

In this sub-section, the validity of the EMT is tested for quartz nanowires of a smaller diameter. Figure 5 shows the spectral energy density emitted by an array of nanowires with diameter D=20 nm, height H=20 nm at distance $z_0=100$ nm above the array. The array has a filling factor of f=0.09 (d=40 nm) in Fig. 5(a) and a filling factor of f=0.30 (d=12 nm) in Fig. 5(b). In both cases, $L/z_0 \ll \pi$ such that the EMT is said to be valid. However, as it is seen from Fig. 5, none of the EMT models accurately predicts the magnitude and the spectrum of the energy density. The nanowires in Fig. 5(a) are much smaller than the thermal wavelength, the nanowire spacing as well as the observation distance such that the nanowires can be modeled as cylindrical dipoles. Even in this simple case, the EMT is not able to accurately model near-field thermal emission by the array.

E. Effect of material

The validity of the EMTs for predicting near-field thermal emission by nanowire arrays made of a plasmonic material, namely ITO, is tested in this section. The nanowires have a diameter D=100 nm and a height of H=200 nm, and the filling factor of the array is f=0.3. The dielectric function of the ITO is modeled using the Drude equation as $\varepsilon_{ITO}=\varepsilon_{\infty}-\omega_p^2/(\omega^2+i\gamma\omega)$, where $\varepsilon_{\infty}=3.95$, $\omega_p=2$ eV, and $\gamma=0.11$ eV. The energy density as computed using the T-DDA is compared with the EMTs results at an observation distances of $z_0=50$ nm in Fig. 6(a) and $z_0=100$ nm in Fig. 6(b). As it can be seen from these figures, the MG EMT provides acceptable estimation of the energy density particularly at shorter wavenumbers, while the BR EMT significantly overestimates thermal emission at shorter frequencies. Both EMTs converge to the same results at higher wavenumbers. Additionally, as the distance increases to $z_0=100$ nm, the EMT results get closer to the T-DDA simulations. While the total energy density precited by the MG EMT at $z_0=50$ nm is different from the T-DDA by 31%, the EMT results differ from the T-DDA solution only by 18%. This observation is consistent with previous findings that modeling resonant materials, such as quartz, using the EMTs is more challenging than non-resonant materials such as ITO [55,56].

IV. CONCLUSIONS

The validity of the MG and BR EMTs for modeling near-field thermal emission by nanowire arrays was inspected. Near-field energy density emitted by various quartz nanowires was computed using the EMTs and was compared to numerical simulations using the T-DDA. It was concluded that the EMT cannot accurately predict the energy density magnitude and spectrum for quartz nanowires. Although it is assumed that the EMT is valid when $\frac{L}{z_o} < \pi$, it was shown that this theory deviates significantly from the T-DDA when $\frac{L}{z_o} < 1$. Among the two theories, the MG EMT agrees the most with the T-DDA. The MG EMT predictions are closest to the T-DDA simulations when

 $1 < \frac{L}{z_o} < \pi$. For the ITO nanowires, which do not support any resonances in the infrared portion of the electromagnetic spectrum, the MG EMT provides an acceptable estimation of energy density. It was also shown that the EMTs cannot capture the variation of near-field thermal emission in lateral directions for any materials which can be very significant.

Acknowledgments

The authors acknowledge support from the National Science Foundation under Grant No. CBET-1804360.

References

- [1] S. A. Biehs, M. Tschikin and P. Ben-Abdallah, Phys. Rev. Lett. 109, 104301 (2012).
- [2] G. D'Aguanno, N. Mattiucci, A. Alù, C. Argyropoulos, J. V. Foreman, and M. J. Bloemer, Opt. Express 20, 9784 (2012).
- [3] X. J. Wang, J. L. Abell, Y-P. Zhao and Z. M. Zhang, Appl. Opt. 51, 1521 (2012).
- [4] S. Basu and L. Wang, Appl. Phys. Lett. 102, 053101 (2013).
- [5] X. L. Liu, L. P. Wang and Z. M. Zhang, J. Heat Transf. 135, 061602 (2013).
- [6] X. L. Liu, R. Z. Zhang and Z. M. Zhang, Appl. Phys. Lett. 103, 213102 (2013).
- [7] C. Simovski, S. Maslovski, I. Nefedov and S. Tretyakov, Opt. Express 21, 14988 (2013).
- [8] H. Wang, X. Liu, L. Wang and Z. M. Zhang, Int. J. Therm. Sci. 65, 62 (2013).
- [9] S. Lang, M. Tschikin, S. A. Biehs, A. Y. Petrov and M. Eich, Appl. Phys. Lett. 104, 121903(2014).

- [10] X. L. Liu, R. Z. Zhang and Z. M. Zhang, Int. J. Heat Mass. Transf. 73, 389 (2014).
- [11] X. L. Liu, R. Z. Zhang and Z. M. Zhang, ACS Photonics 1, 785 (2014).
- [12] J. Y. Chang, S. Basu and L. Wang, J. Appl. Phys. 117, 054309 (2015).
- [13] J. Y. Chang, Y. Yang and L. Wang, Int. Int. J. Heat Mass. Transf. 87, 237 (2015).
- [14] R. Z. Zhang, X. Liu and Z. M. Zhang, AIP Adv. 5, 053501 (2015).
- [15] X. J. Hong, J. W. Li, T. B. Wang, D. J. Zhang, W. X. Liu, Q. H., Liao, T. B. Yu and N. H. Liu, Jpn. J. Appl. Phys. 57, 045001 (2018).
- [16] Z. Shen, H. Wu and H. Wang, Appl. Sci. 8, 2023 (2018).
- [17] H. Wang, D. Qi and H. Wu, J. Photonics Energy 9, 015501 (2019).
- [18] W. B. Zhang, C. Y. Zhao and B. X. Wang, Phys. Rev. B 100, 075425 (2019).
- [19] J. Y. Chang, P. Sabbaghi, Y. S. Weng, Y. B. Chen and L. Wang, J. Heat Transfer 142(7) (2020).
- [20] J. C. Maxwell-Garnett, Philos. Trans. R. Soc. Lond. B 203, 385 (1904).
- [21] T. C. Choy, *Effective Medium Theory: Principles and Applications* 2 ed. (Oxford University Press, New York, 2016).
- [22] V. A. Markel, J. Opt. Soc. Am. A 33(7), 1244-56 (2016).
- [23] D. A. G. Bruggeman, Ann. Phys. (Leipzig) 24, 636 (1935).
- [24] Y. Guo and Z. Jacob, Opt. Express 21, 15014 (2013).
- [25] Y. Guo and Z. Jacob, J. Appl. Phys. 115, 234306 (2014).

- [26] X. L. Liu, T. J. Bright and Z. M. Zhang, J. Heat Transfer 136, 092703 (2014).
- [27] M. Tschikin, S. A. Biehs, P. Ben-Abdallah, S. Lang, A. Y. Petrov and M. Eich, J. Quant. Spectrosc. Radiat. Transf. 158, 17 (2015).
- [28] S. A. Biehs and P. Ben-Abdallah, Z. Naturforsch. A 72, 115 (2017).
- [29] Y. Yang, J. Y. Chang, P. Sabbaghi and L. Wang, J. Heat Transfer 139, 052701 (2017).
- [30] B. Zhao, B. Guizal, Z. M. Zhang, S. Fan and M. Antezza, Phys. Rev. B 95, 245437 (2017).
- [31] M. Lim, J. Song, S. S. Lee and B. J. Lee, Nat. Commun. 9, 4302 (2018).
- [32] H. Iizuka and S. Fan, Phys. Rev. Lett. 120, 063901 (2018).
- [33] J. E. Pérez-Rodríguez, G. Pirruccio and R. Esquivel-Sirvent, Phys. Status Solidi B 257, 1900498 (2020).
- [34] X. Liu, B. Zhao and Z. M. Zhang, Phys. Rev. A 91, 062510 (2015).
- [35] X. Liu and Z. M. Zhang, ACS Photonics 2, 1320 (2015).
- [36] X. Liu and Z. M. Zhang, Appl. Phys. Lett. 107, 143114 (2015).
- [37] Y. Yang and L. Wang, Phys. Rev. Lett. 117, 044301 (2016).
- [38] Y. Yang, P. Sabbaghi and L. Wang, Int. J. Heat Mass Transf. 108, 851 (2017).
- [39] A. Didari and M. P. Mengüç, Opt. Express 23, A547 (2015).
- [40] A. Didari and M. P. Mengüç, Opt. Express 23, A1253 (2015).
- [41] A. Didari and M. P. Mengüç, J. Quant. Spectrosc. Radiat. Transf. 197, 95 (2017).

- [42] V. Fernández-Hurtado, F. J. García-Vidal, S. Fan and J. C. Cuevas, Phys. Rev. Lett. 118, 203901 (2017).
- [43] H. Yu, Y. Duan and Z. Yang, Int. J. Heat Mass Transf. 123, 67 (2018).
- [44] M. S. Mirmoosa, F. Rüting, I. S. Nefedov and C. R. Simovski, J. Appl. Phys. 115, 234905(2014).
- [45] S. M. Rytov, Y. A. Kravtsov and V. Tatarskii, *Principles of Statistical Radiophysics 3: Elements of Random Fields* (Springer, New York, 1989).
- [46] C.A. Balanis, *Advanced Engineering Electromagnetics* 2 ed. (John Wiley & Sons, Inc., New Jersey, 2012).
- [47] A. O. Silva and J. C. Costa, J. Microw. Optoelectron. Electromagn. Appl. 13, 10 (2014).
- [48] M. Francoeur, M. P. Menguc and R. Vaillon, J. Quant. Spectrosc. Radiat. Transfer 110, 2002 (2009).
- [49] M. Francoeur, M. P. Menguc and R. Vaillon, J. Phys. D: Appl. Phys. 43, 075501 (2010).
- [50] S. Edalatpour and M. Francoeur, J. Quant. Spectrosc. Radiat. Transfer 133, 364 (2014).
- [51] S. Edalatpour, M. Čuma, T. Trueax, R. Backman and M. Francoeur, Phys. Rev. E 91, 063307 (2015).
- [52] S. Edalatpour, Phys. Rev. E 99, 063308 (2019).
- [53] L. Tsang, J. A. Kong, K. Ding and C. O. Ao, *Scattering of Electromagnetic Waves: Numerical Simulations* (John Wiley & Sons, Inc., New York, 2002).

- [54] C. F. Bohren and D. R. Huffman, *Absorption and Scattering of Light by Small Particles* (Wiley, New York, 1998).
- [55] P. Sheng, *Introduction to Wave Scattering, Localization and Mesoscopic Phenomena* 2 ed. (Springer, 2006).
- [56] X. Zhang and Y. Wu, Sci. Rep. 5, 7892 (2015).

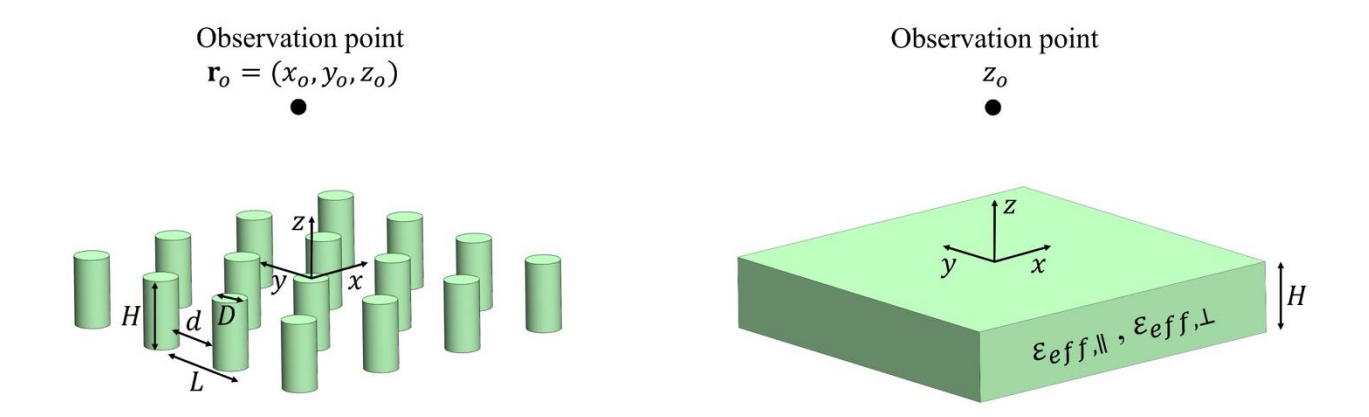


Figure 1 – (a) A periodic array of nanowires with diameter D, height H, and interwire distance d thermally emits in the free space. (b) In the EMT, the array is modeled as a homogeneous thin film with height H and effective parallel and perpendicular dielectric functions $\varepsilon_{eff,\parallel}$ and $\varepsilon_{eff,\perp}$, respectively.

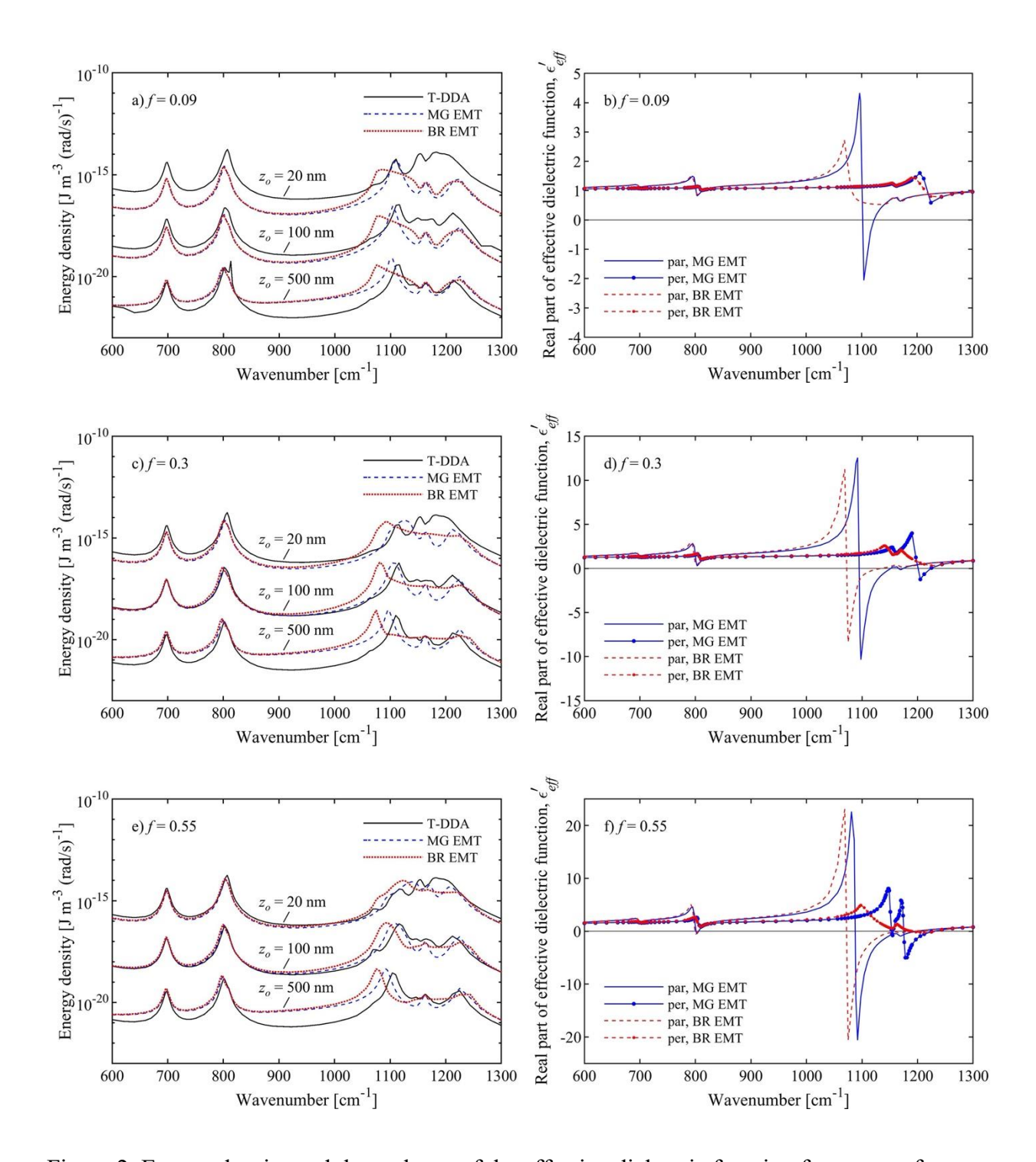


Figure 2. Energy density and the real part of the effective dielectric function for arrays of quartz nanowires with D = 100 nm, H = 20 nm, and three filling factors of f = 0.09, 0.30, and 0.55. The arrays emit at 400 K.

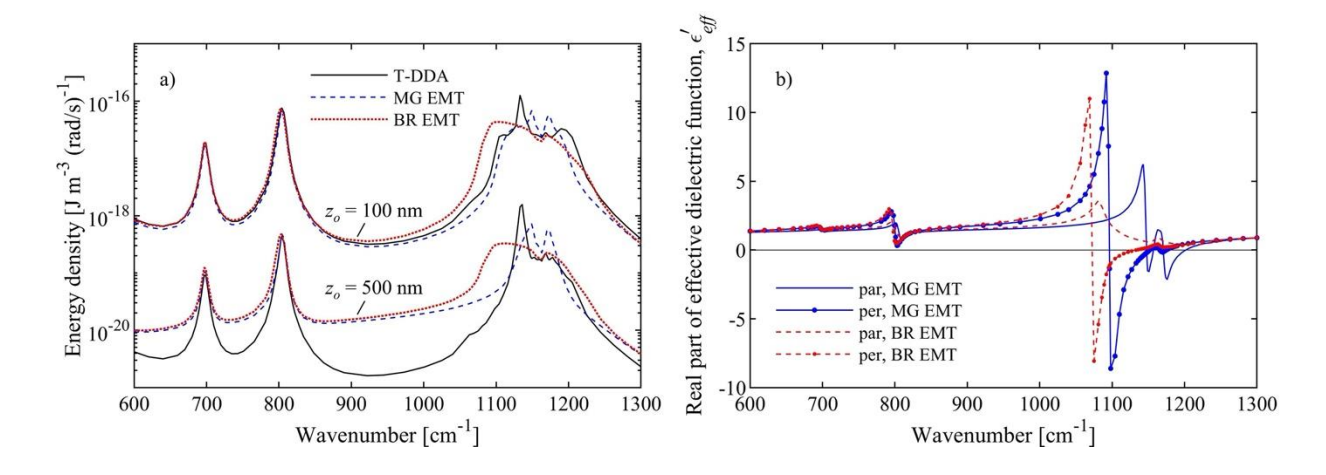


Figure 3. (a) Energy density emitted by an array of quartz nanowires with D = 100 nm, H = 200 nm, and f = 0.30 at two observation distances z_o of 100 nm and 500 nm. (b) The real part of the effective dielectric function of the array as predicted by the MG and BR EMTs.

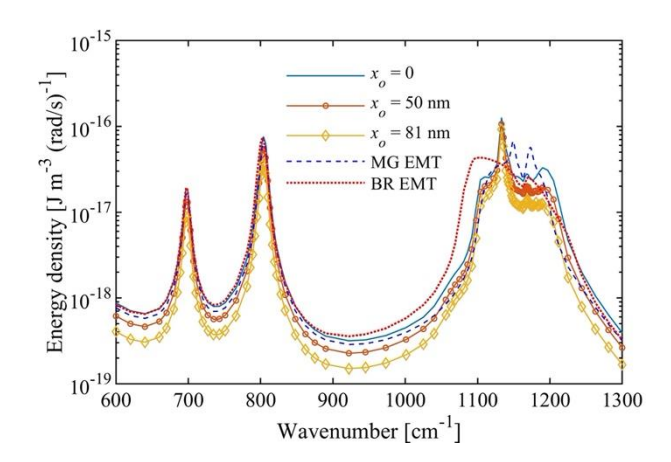


Figure 4. Energy density emitted by an array of quartz nanowires with D = 100, H = 200 nm, and f = 0.30 at a distance z_o of 100 nm and three lateral distances x_o of 0 nm, 50 nm, and 81 nm. $y_o = 0$.

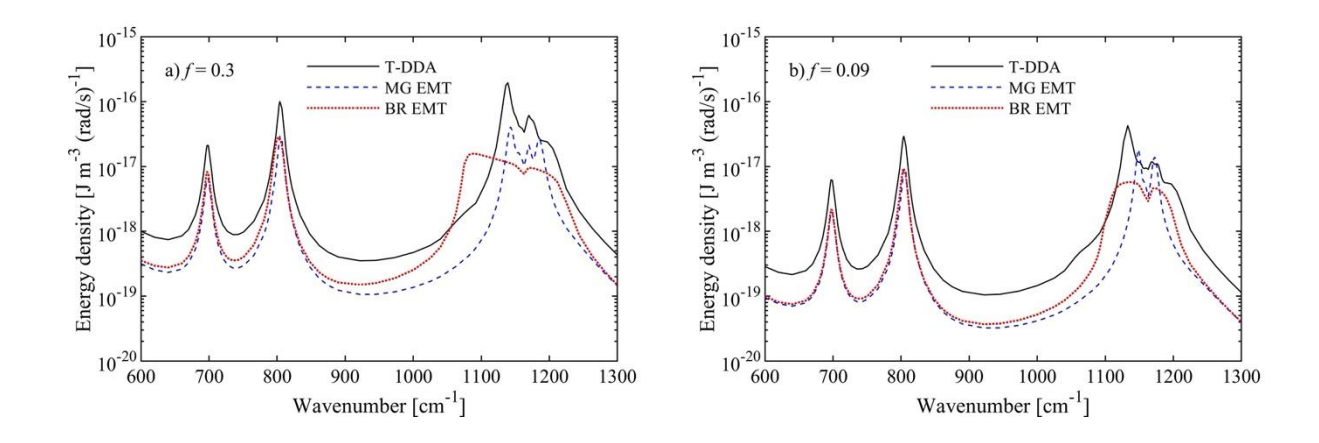


Figure 5. The energy density emitted by arrays of quartz nanowires of diameter D=20 nm and height H=20 nm at an observation distance of $z_0=100$ nm. The filling factor f is equal to 0.3 in Panel (a) and 0.09 in Panel (b).

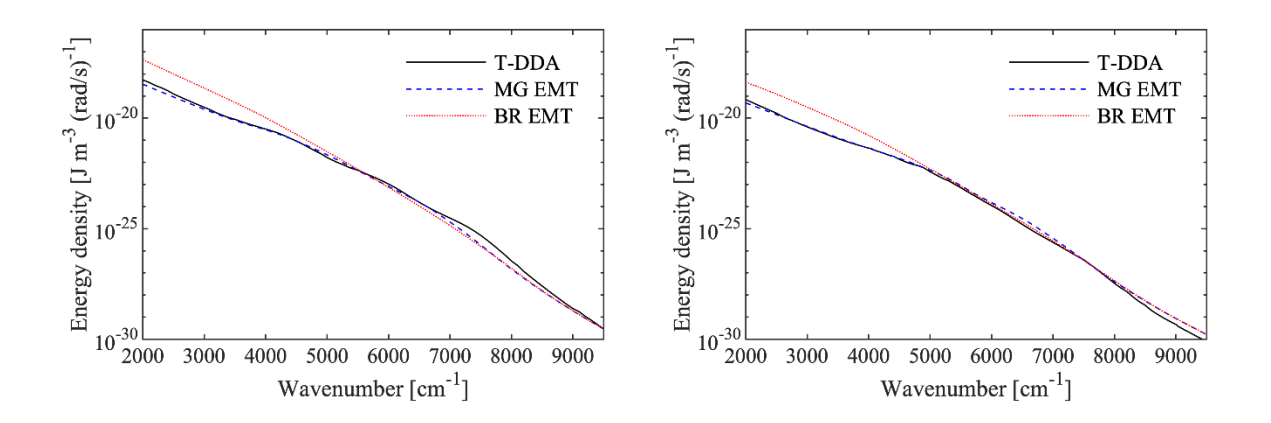


Figure 6. The energy density emitted by an array of ITO nanowires of diameter D=100 nm, height H=200 nm, and filling factor f=0.3 at an observation distance of (a) $z_o=50$ nm and (b) $z_o=100$.